Supplementary Information (SI) for RSC Advances.

Supplementary data

Combined antimicrobial and anti-inflammatory properties of electrospun PCL nanohybrids infused with metal- turmeric oleoresin and metal-curcuminoids.

SI 1: Preparation of samples for egg albumin assay

For the assay, each sample contained the following components: 0.2 mL of fresh egg albumin, 2.8 mL of phosphate-buffered saline (PBS) at pH 6.4, and 2 mL of the sample dispersed in 0.2% DMSO at various concentrations. The concentrations of the test samples ranged from 5000 ppm to 312.5 ppm (5 mg/mL to 0.3125 mg/mL).

The absorbance of the samples was first measured at 680 nm before heating to eliminate the influence of sample color. Following this, the samples were incubated at 37°C for 30 minutes to facilitate initial interactions. They were then heated in a water bath at 70°C for 5 minutes to induce denaturation of the egg albumin. After heating, the mixtures were allowed to cool to room temperature, and the absorbance was measured again at 680 nm.

For the negative control, the assay included 0.2 mL of fresh egg albumin, 2 mL of 0.2% DMSO, and 2.8 mL of PBS. Prednisolone was used as the positive control for the assay. The percentage inhibition was calculated using the appropriate formula.[33]

Here, represent the respective absorbance of negative control, absorbance of sample after heating, and absorbance of the sample before heating at 680 nm wavelength.

SI 2: Characterization of synthesized metallic nanoparticles

An X-ray diffraction (XRD) analysis was performed to investigate the crystal structure of synthesized metallic nanoparticles. Data were acquired using a Rigaku Ultima IV diffractometer equipped with a 3 kW sealed X-ray tube, operated at 40 kV and 30 mA. Nanoparticles were scanned over a 2θ range of 20° to 80° at scan rate of $1°min^{-1}$ with 0.002° step width. For analyzing the functional groups, Fourier transform infrared (FTIR) analysis was carried out using the KBr pellet method with a Bruker Vertex 80 instrument, covering the spectral range of 400 cm^{-1} to 4000 cm^{-1}. Additionally, Raman spectroscopic analysis was conducted with a Thermo Scientific DXR instrument, employing a fine-power of laser within the range of 250 cm^{-1} – 2500 cm^{-1}.

The surface morphological features of metallic nanoparticles were examined using scanning electron microscopy (SEM) with a ZEISS model, utilizing the secondary electron method at an accelerated voltage of 10 kV. The average particle diameter and its distribution were calculated using Image J software (Image J 1.51). Energy dispersive x-ray spectrometry analysis (EDX) was performed alongside with the SEM to observe the distribution of relevant metal atom throughout the sample.

The optical band gap energy (Eg) of trimetallic nanohybrid was determined using UV-Vis diffuse reflectance spectrometry. This energy represents the minimum energy required to excite an electron from the valence band to the conduction band. The Tauc plot, which establishes a relationship between absorption coefficient and photon energy, was used to determine the Eg.[36]

SI 3: Well-diffusion assay of metallic nanoparticles combined with curcuminoids and turmeric oleoresins

The media and micropipette tips were sterilized by autoclaving at 121°C (15 bar pressure) for 15 minutes, while other glassware was sterilized in a hot air oven at 160°C for 2 hours. Next, 25 mL of Mueller-Hinton agar (MHA) was poured into each disposable petri dish and allowed to solidify. Once solidified, to obtain a confluent growth, a sterile cotton swab was first dipped into each microbial suspension and then gently streaked across the surface of the agar in a zigzag pattern, ensuring even distribution. The swab was then rotated to cover the entire plate, moving back and forth to spread the microorganisms. The microbial suspensions were freshly prepared from cultures of the selected microbes. Sterile pipette tips were used to create wells in the agar, and the bottoms of the wells were sealed with 1–2 drops of MHA, which was allowed to dry. Subsequently, 50 µL of each metallic nanohybrid dispersion (at a concentration of 100 mg/mL) was added to the respective wells. The plates were then incubated at 37°C for 24 hours. After incubation, the zone of inhibition surrounding each well was measured using a Netillin Zone Reader (USA). All experiments were performed in triplicate and followed the guidelines set by the Clinical and Laboratory Standards Institute (CLSI).

SI 4: **Quantification of oleoresin and curcuminoids crystals using UV-vis spectrometric analysis and the characterization**

A calibration curve for reference curcuminoids was created by plotting absorbance values against the corresponding concentrations of curcuminoids in ethanol. This enabled the quantitative determination of curcuminoids content. The slope, intercept, correlation coefficient (R^2), and regression equation were determined, resulting in the linear equation: $y = 0.1013x - 0.0362$, where x represents the concentration and y represents absorbance. The correlation coefficient (R^2) was found to be 0.997, indicating a strong linear relationship within the concentration range of 2.5 mg/mL to 10.00 mg/mL. The average absorbance value for turmeric oleoresin was measured at 0.214, while the absorbance value for curcuminoid crystals was 0.446 at a wavelength 427 nm. The estimated percentage purity of the turmeric oleoresin and curcuminoid crystals samples was found to be 49.44 ± 0.53% and 95.12 ± 0.43% respectively, and these values align well with those reported in the literature.[48]

Characterization of oleoresin and curcuminoids

The crystalline phase of curcuminoids was identified using powder X-ray diffraction (PXRD), as illustrated in Figure S3(a). The PXRD pattern for curcuminoids displays sharp, well-defined peaks within the 2θ range of 10 to 30 degrees, indicating a high degree of crystallinity in the curcuminoid

sample. The observed diffraction pattern was indexed according to JCPDS number 9-816, confirming the crystalline phase of the curcuminoids. Similar findings were reported by Z. Sayyar and H. Jafarizadeh Malmiri[49], highlighting a total of 10 peaks within the 10 to 30 degrees 2θ range.

The structure of turmeric oleoresin and curcuminoids crystals were further supported and compared with reference curcuminoids through FTIR analysis as shown in Figure S3(b). The functional groups and their corresponding peak positions were identified using FTIR analysis. The FTIR spectra exhibit stretching vibrations at 1629 cm^{-1} and 1638 cm^{-1}, primarily attributed to the overlapping stretching vibrations of alkenes (C=C) and carbonyl (C=O) groups. A broad peak around 3450 cm^{-1} is observed, corresponding to the stretching vibrations of hydroxyl (OH) groups. Additionally, there is a band at 1513 cm^{-1} attributed to mixed vibrations, including the stretching carbonyl bond, in plane bending vibrations associated with aliphatic (δ CC-C, δ CC=O) and stretching vibrations related to aromatic (δ CC-H) bonds in both keto and enol configuration of curcumin. Furthermore, a peak at 1284 cm^{-1} is attributed to the bending vibrations of the υ(CO) phenolic band.[50] The band appears around 2360 cm^{-1} is mainly due to CO adsorption on the surface from the CO_2 in the atmosphere.

SI 5: Characterization of synthesized metallic nanoparticles

As shown in Figure S4(a)(i), the XRD pattern of the synthesized silver (Ag) reveals several distinct peaks that correspond to specific crystal planes. The observed planes (111), (200), (220), (311), and (222) indicate that Ag has a face-centered cubic (fcc) structure. The sharpness and intensity of these peaks suggest that the sample is well-crystallized, with the high intensity of the (111) peak indicating a preferred orientation in that direction. The resolved peaks align well with the JCPDS file no. 04-0783, which corresponds to the crystalline structure of silver.

Figure S4(a)(ii) illustrates the XRD pattern for the synthesized copper (Cu) combined with copper(I) oxide (Cu_2O). Copper is easily oxidized in the presence of a small amount of oxygen, which leads to a greater formation of Cu_2O rather than metallic Cu. The XRD graph highlights the dominance of Cu_2O (JCPDS 05-0667) in the sample, alongside some peaks that correspond to metallic Cu (JCPDS 04-0836). The identified planes (110), (111), (200), (211), (220), (311), and (222) indicate the cubic structure of Cu_2O. Additionally, several peaks corresponding to the (111), (200), and (220) planes suggest the presence of the fcc structure in metallic Cu.

Figure S4(a)(iii) presents the XRD pattern for synthesized nickel (Ni), where the resolved peaks match well with JCPDS file no. 03-1051. The peaks observed at 44.49°, 51.88°, and 76.34° correspond to the (111), (200), and (220) crystallographic planes, respectively, confirming that the Ni nanoparticles also exhibit a face-centered cubic structure. The well-resolved peaks further validate the crystalline nature of the synthesized Ni sample.[51-53]

The synthesis of nanoparticles were further supported by FTIR analysis, which confirm the presence of functional groups, peak positions, and relevant peak shifts. As shown in Figure S4(b), there is a broad peak around 3450 cm^{-1} in all spectra, attributed to the stretching vibration of O-H group in absorbed water. The spectrum of pure ascorbic acid, illustrated in Figure S4(b)(iv), revealed the stretching vibration of the C=C double bond at 1674 cm^{-1}. This peak shifts to the left in metal nanohybrids, resulting in a blue shift. In pure ascorbic acid, the peak corresponding to the enol hydroxyl group at 1320 cm^{-1} shifts to the right in the metal nanohybrid, causing a red shift. In the case of Ag NPs, these peaks have moved to 1630 cm^{-1} and 1384 cm^{-1} (Figure S4(b)(i)). For Cu NPs, the shifts are to1628 cm^{-1} and to 1384 cm^{-1} (Figure S4(b)(ii)), while in Ni NPs, the peak shift to 1634 cm^{-1} and to 1384 cm^{-1} (Figure S4(b)(iii)). Additionally, in the fingerprint region of the metal nanoparticles, a peak at 619 cm^{-1} in Cu NPs is observed, which corresponds to the vibration of the Cu-O bond, confirming the presence of Cu-O alongside the copper metal. Considering these characteristic peaks and their respective shifts, it can be concluded that the synthesis of metal nanohybrids capped with ascorbic acid was successfully achieved.[54]

Figure S4(c) depicts the Raman spectra of synthesized Ag, Cu, Ni and ascorbic acid. As shown in Figure S4(c)(iv), ascorbic acid exhibits strong Raman scattering lines at 625 cm^{-1}, 818 cm^{-1}, 1024 cm^{-1}, 1124 cm^{-1}, 1293 cm^{-1}, 1487 cm^{-1}, and 1651 cm^{-1}. These peaks correspond to various vibrations: OH out-of-plane deformation, C-C ring stretching, C-O-H bending, C-O-C stretching and ring deformation, C-O-H bending (twisting), C-H bending, and C=C stretching, respectively.[55] In the metal nanohybrids, these peaks have shifted, confirming the successful capping during the synthesis of metal nanohybrids. The peak at 1487 cm^{-1} in pure ascorbic acid shifts in Ag NPs to 1477 cm^{-1} (Figure S4(c)(i)), to 1501 cm-1 in Cu NPs (Figure S4(c)(ii)), and to 1484 cm^{-1} in Ni NPs (Figure S4(c)(iii)). For pure ascorbic acid, the peaks at 818 cm^{-1}, 1293 cm^{-1}, and 1024 cm^{-1}, shift to 810 cm^{-1}, 1299 cm^{-1}, and 1047 cm^{-1} in Ag NPs and to 816 cm^{-1} and 1299 cm^{-1} in Ni NPs, respectively. However, these peaks cannot be observed in Raman spectrum of Cu NPs due to differences in intensity; the broad peak at 1501 cm^{-1} in Cu NPs may mask them. Additionally, the peaks at 516 cm^{-1}, and 614 cm^{-1} in Cu NPs are associated with metal-oxygen bonds, further confirming the formation of oxides in Cu sample.

Materials that possess a visible light-active band gap can be excited by visible light, leading to the generation of electron-hole pair. This process is essential for producing reactive oxygen species (ROS). The ability to efficiently harness visible light for the generation of reactive oxygen species (ROS) is a vital feature of these nanoparticles. This characteristic significantly contributes to their effectiveness in various fields, including antimicrobial applications where they can eliminate harmful microorganisms, environmental cleanup efforts aimed at removing pollutants, and photocatalytic processes that facilitate chemical reactions using light energy.

In this study, the optical band gap energy (Eg) was evaluated by combining equal proportions of three different metal nanohybrids to create a trimetallic nanohybrid. Using UV-Vis diffuse reflectance spectrometry, the Eg for the trimetallic nanohybrid (Figure S4(d)) was estimated. The

calculated Eg value was 2.03 eV, indicating that this trimetallic nanohybrid exhibits visible light-active ROS generation, which is vital for its antimicrobial functionality.

After the structural characterization, the metal nanoparticles were analyzed morphologically using SEM imaging. Figure S4(e) shows that the nanoparticles are spherical in shape. Using Image J software, the mean particle diameter was calculated. The recorded mean particle diameter for Ag NPs (Figure S4 (f)(i)) was 200 ± 7.86 nm, and for Cu and Cu_2O NPs (Figure S4(f)(ii)) it was 167 ± 5.24 nm, and for Ni NPs (Figure S4 (f)(iii)) it measured 88 ± 7 nm. Notably, Ag and Cu and Cu_2O NPs exhibited a much larger particle diameter due to some aggregate formation among the nanoparticles. This phenomenon occurs because certain metal nanoparticles can act as nuclei for the growth of other nanoparticles within the sample, leading to agglomeration. This agglomeration is driven by the attractive van der Waals forces between the crystals.[56]

The Energy Dispersive X-ray (EDX) analysis of the synthesized nanoparticles revealed valuable information regarding the elemental composition of the samples (Figure S5). In the silver (Ag) sample, the weight percentage (wt.%) of silver was found to be 84.77%, while the atomic percentage (at.%) was 42.86%. This suggests that silver dominates the sample in terms of mass, but the atomic percentage is relatively lower due to the higher atomic weight of silver compared to oxygen (O) and carbon (C), which were also present. The presence of carbon is likely attributed to the capping agent used during synthesis, a common practice to stabilize nanoparticles and prevent agglomeration. Oxygen may have been incorporated through surface oxidation of the silver nanoparticles, which is typical upon exposure to atmospheric oxygen.

In the copper (Cu) sample, the EDX analysis indicated a weight percentage of 79.18% and an atomic percentage of 48.76%. The atomic percentage of copper is notably higher than its weight percentage, which can be explained by the relatively lower atomic mass of copper compared to silver, leading to a greater atomic contribution. As with the silver sample, the presence of oxygen and carbon suggests surface oxidation of copper nanoparticles to species such as CuO or Cu_2O and the influence of the capping agent. The significant atomic percentage of copper confirms that the sample is primarily composed of copper, and surface oxidation is likely to have occurred on the nanoparticle surfaces.

For the nickel (Ni) sample, the EDX analysis showed a weight percentage of 71.95% and an atomic percentage of 43.82%. Similar to the copper sample, the atomic percentage of nickel is higher than its weight percentage, reflecting the heavier atomic mass of nickel relative to carbon and oxygen. Traces of sodium (Na) and chlorine (Cl) were also detected, which are likely residuals from the precursor chemicals used in the synthesis process. These elements are present in low concentrations and may not significantly affect the properties of the nanoparticles, although they suggest that additional purification steps may be necessary to remove any remaining precursor contaminants. The presence of oxygen in the nickel sample suggests that a nickel oxide (NiO) layer may have formed on the surface of the nanoparticles, as is common with transition metals exposed to air.

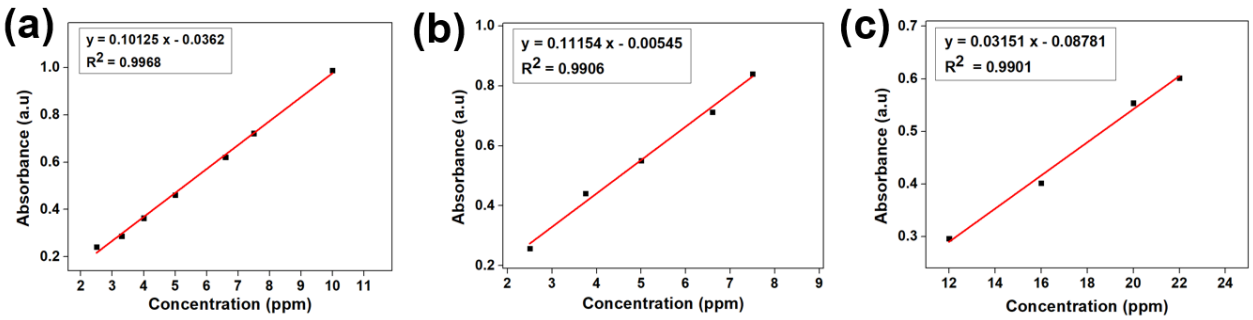

Figure S1: Quantification of oleoresin and curcuminoids crystals by UV-vis spectrometric analysis. Calibration plots of curcuminoids in a). ethanol b). acetone and c). PBS : ethanol (1:1) solution.

Construction of calibration curve for standard curcuminoids

A standard calibration curve was created using a standard solution in the concentration range of 2.5 mg/L to 10 mg/L (or 2.5 ppm to 10 ppm), with ethanol as the solvent. The absorbance of these solutions was measured at 427 nm using UV-vis spectrophotometer.[30] A plot of absorbance versus the concentration of standard curcuminoids was generated to establish the calibration curve. Another two standard calibration curves were also created with acetone, and PBS: ethanol 1:1, at 427 nm in wavelength, for further purposes in this study. Figure.S1presents the standard calibration curves of different solutions.

Preparation of test solutions and sample quantification

Test solutions were prepared by dissolving 20.00 mg of oleoresin/curcuminoids crystals in 100 mL of ethanol. A 1 mL aliquot of the solution was then diluted to 40 mL in a volumetric flask using the ethanol solvent to create a 5 ppm solution. The absorbance of the resulting solution was measured at 427 nm using a UV-vis spectrophotometer. The procedure was repeated three times in order to obtain an average absorbance value at 427 nm.

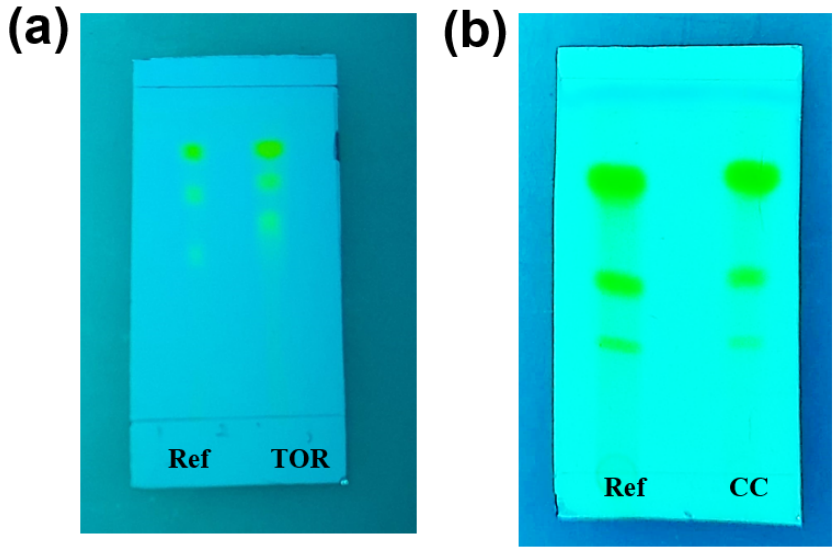

Figure S2: (a) TLC for turmeric oleoresin (TOR) and (b) TLC for curcuminoids crystals (CC): with reference curcuminoids (Ref): spots from solvent front to origin represent curcumin, DMC, and BDMC respectively.

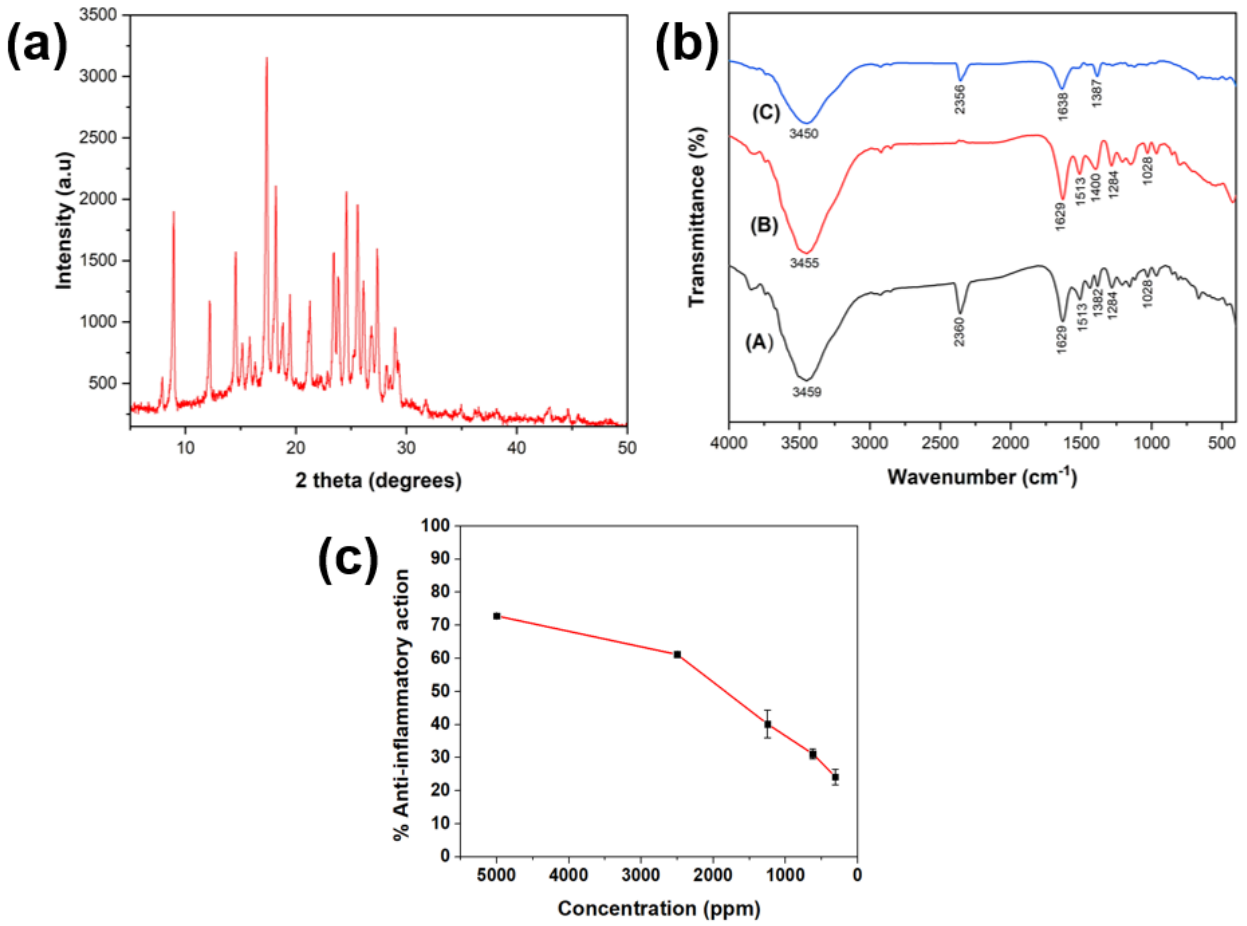

Figure S3: (a) PXRD pattern for curcuminoids, (b) FTIR spectra for (A) reference curcuminoids, (B) curcuminoids crystals, and (C) oleoresin, (c) anti-inflammatory activity of curcuminoids at different concentrations.

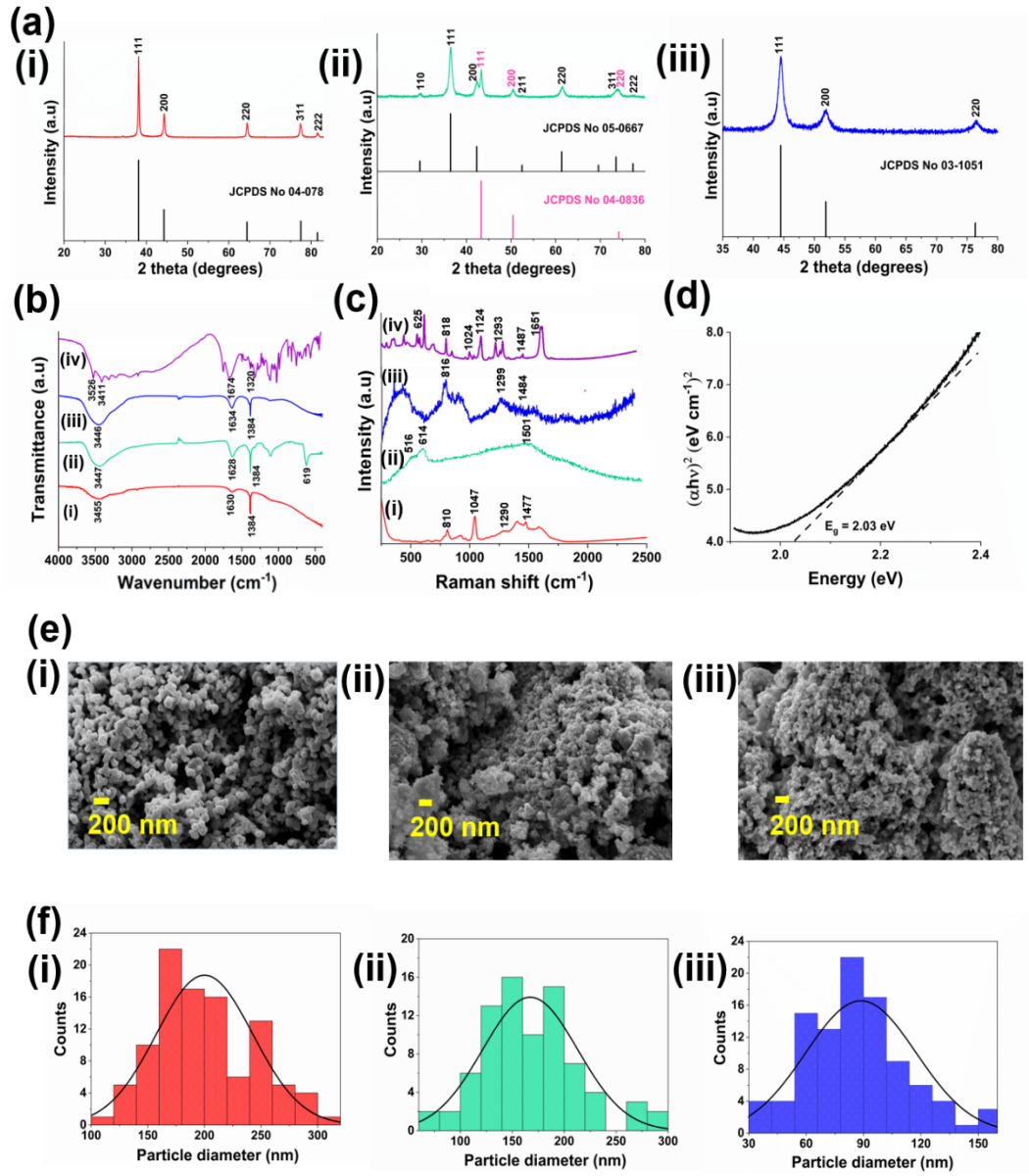

Figure S4: (a) PXRD spectra of (i) Ag NPs, (ii) Cu NPs, (iii) Ni NPs; (b) FTIR spectrum of (i) Ag NPs, (ii) Cu NPs, (iii) Ni NPs, (iv) pure ascorbic acid; (c) Raman spectrum of (i) Ag NPs, (ii) Cu NPs, (iii) Ni NPs, (iv) ascorbic acid; (d) Optical band gap energy of a trimetallic nanohybrid (e) The SEM image of (i) Ag NPs, (ii) Cu NPs, (iii) Ni NPs; (f) Particle diameter distribution of (i) Ag NPs, (ii) Cu NPs, (iii) Ni NPs.

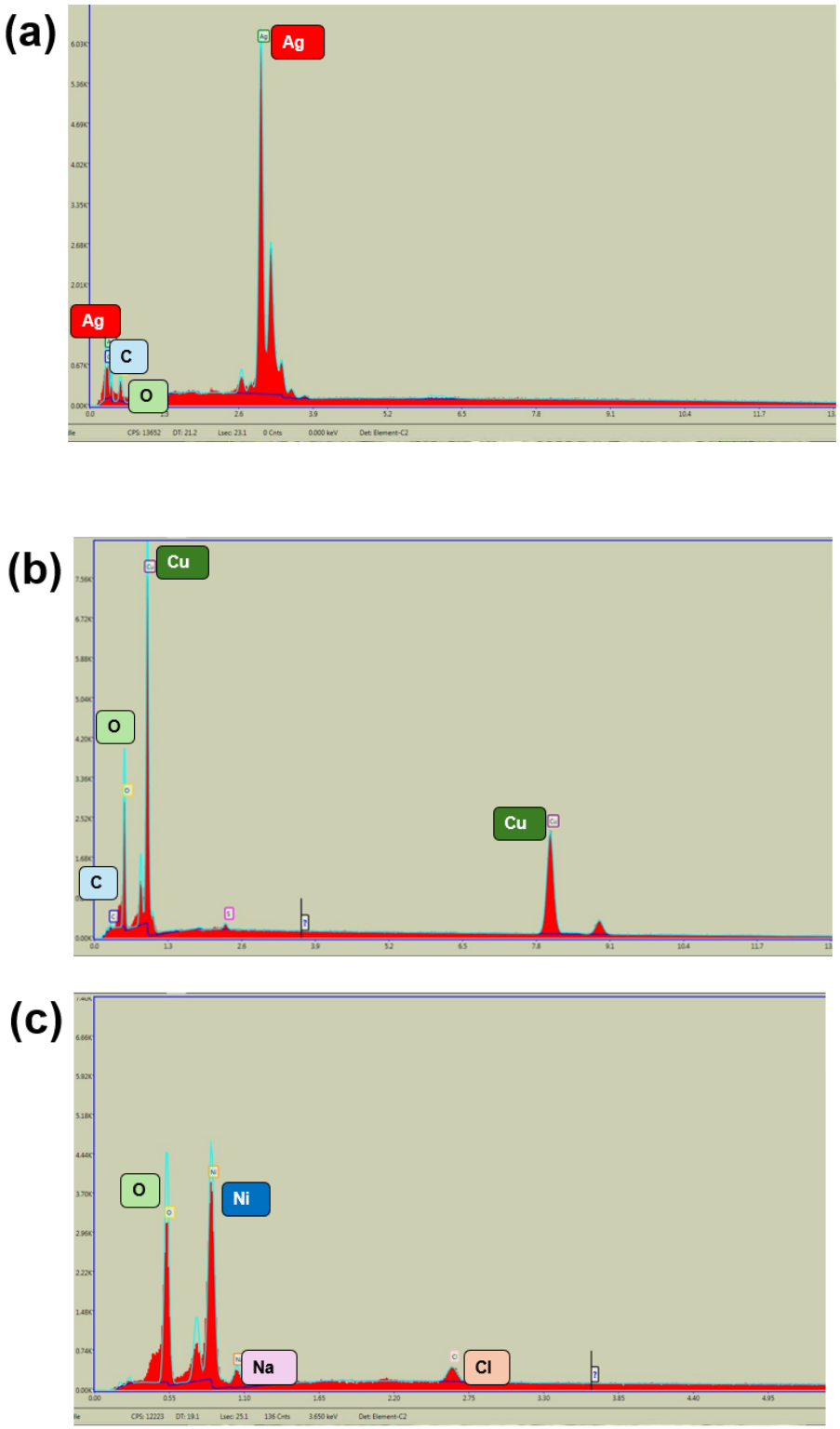

Figure S5: EDX mapping for (a) Ag (b) Cu and (c) Ni nanoparticles.

		Mean (mV)	Area (%)	St Dev (mV)
Zeta Potential (mV): -25.0	Peak 1:	-25.0	100.0	3.80
Zeta Deviation (mV): 3.80	Peak 2:	0.00	0.0	0.00
Conductivity (mS/cm): 0.766	Peak 3:	0.00	0.0	0.00

Result quality : Good

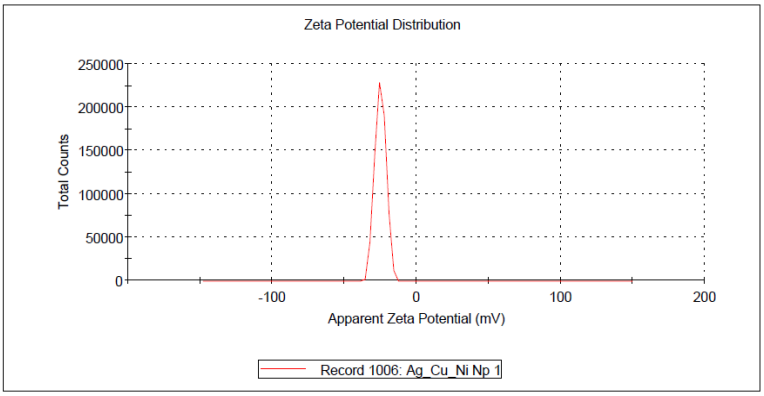

		Mean (mV)	Area (%)	St Dev (mV)
Zeta Potential (mV): -25.1	Peak 1:	-25.1	100.0	4.51
Zeta Deviation (mV): 4.51	Peak 2:	0.00	0.0	0.00
Conductivity (mS/cm): 0.808	Peak 3:	0.00	0.0	0.00

Result quality : Good

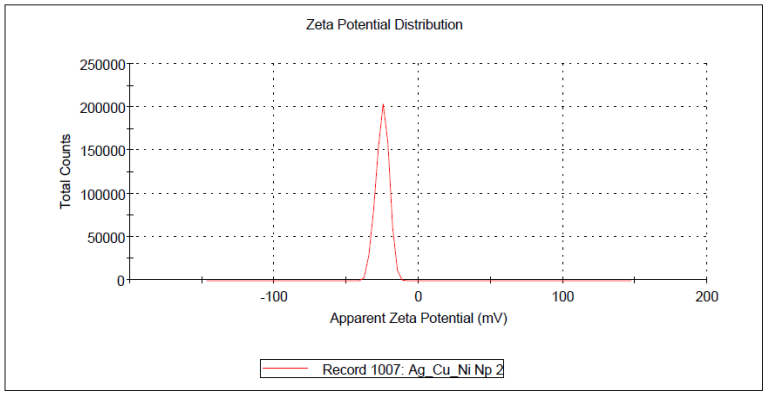

		Mean (mV)	Area (%)	St Dev (mV)
Zeta Potential (mV): -26.0	Peak 1:	-26.0	100.0	4.85
Zeta Deviation (mV): 4.85	Peak 2:	0.00	0.0	0.00
Conductivity (mS/cm): 0.828	Peak 3:	0.00	0.0	0.00

Result quality : Good

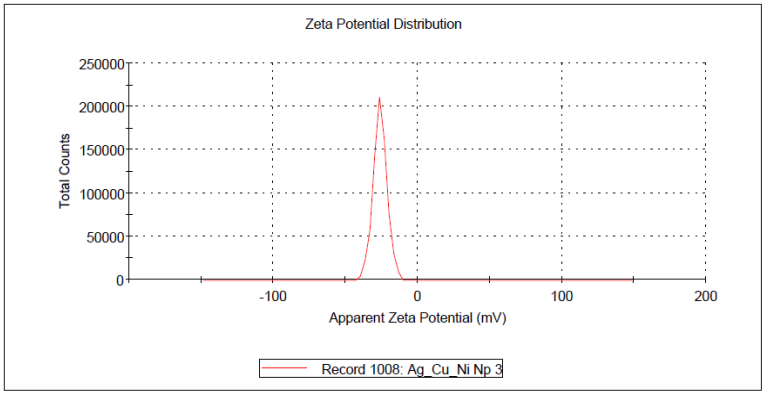

Figure.S6: Zeta potential of analysis of Ag, Cu, and Ni nanoparticle combination in water at room temperature (n=3).

		Size (d.nm):	% Intensity:	St Dev (d.n...
Z-Average (d.nm): 714.5	Peak 1:	825.2	91.4	496.6
PdI: 0.427	Peak 2:	4847	8.6	725.0
Intercept: 0.829	Peak 3:	0.000	0.0	0.000

Result quality : Good

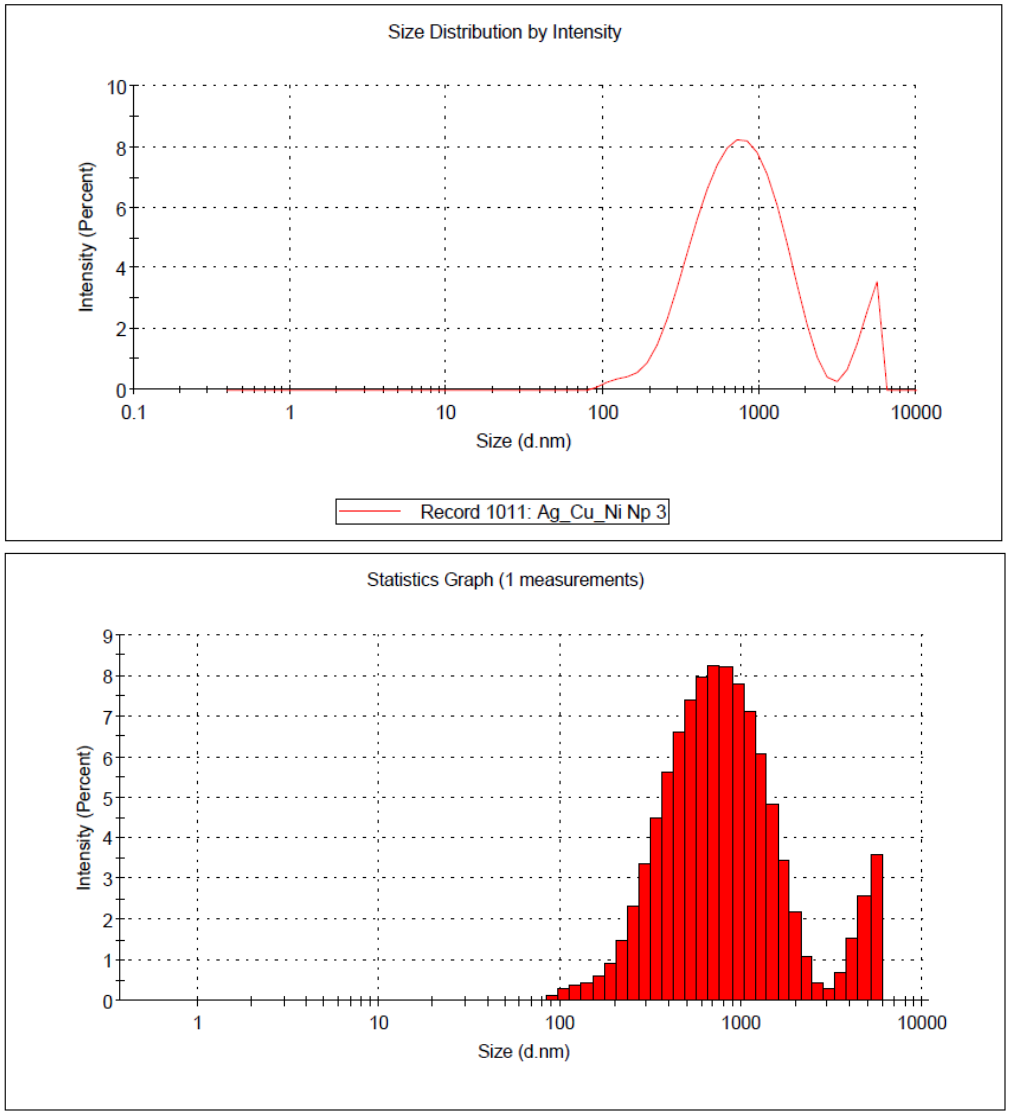

Figure S7: Dynamic light scattering analysis of Ag, Cu, and Ni nanoparticle combination in water.

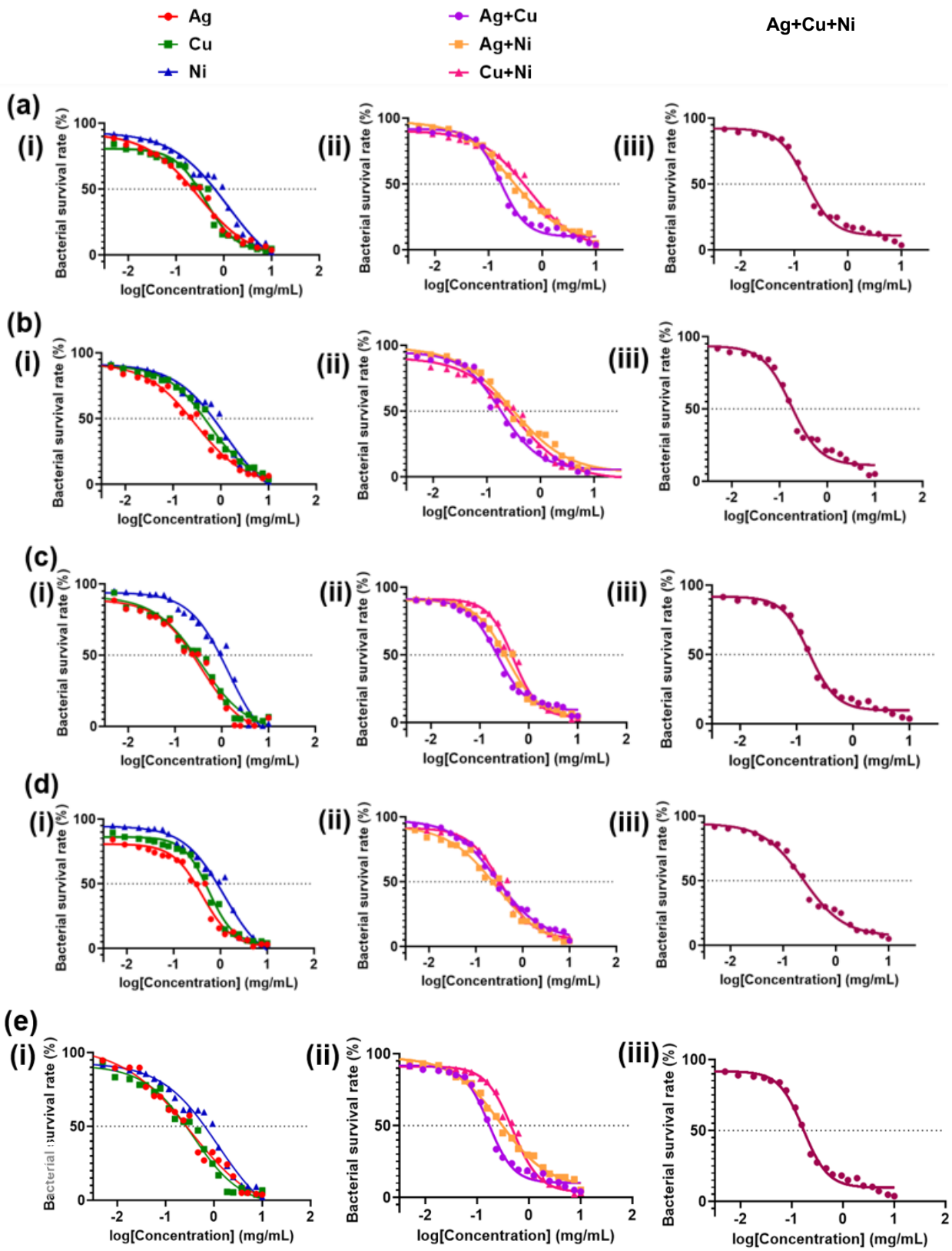
Ag
Cu
Ni
Ag+Cu
Ag+Ni
Cu+Ni
Ag+Cu+Ni
(a)
(b)
(c)
(d)
(e)
(i)
(ii)
(iii)
Bacterial survival rate (%)
log[Concentration] (mg/mL)

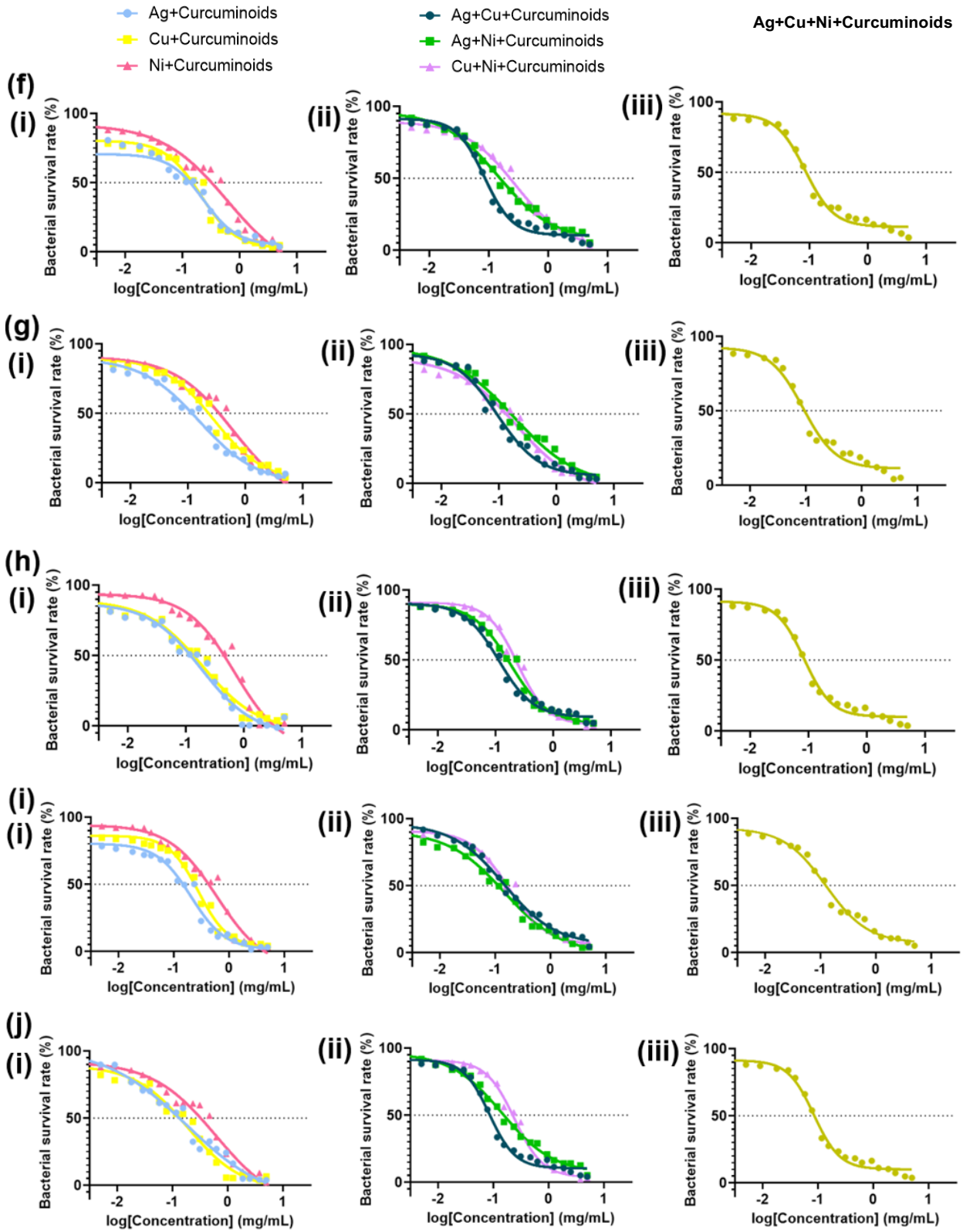
Ag+Curcuminoids
Cu+Curcuminoids
Ni+Curcuminoids
Ag+Cu+Curcuminoids
Ag+Ni+Curcuminoids
Cu+Ni+Curcuminoids
Ag+Cu+Ni+Curcuminoids
(f)
(g)
(h)
(i)
(j)
(i)
(ii)
(iii)
Bacterial survival rate (%)
log[Concentration] (mg/mL)

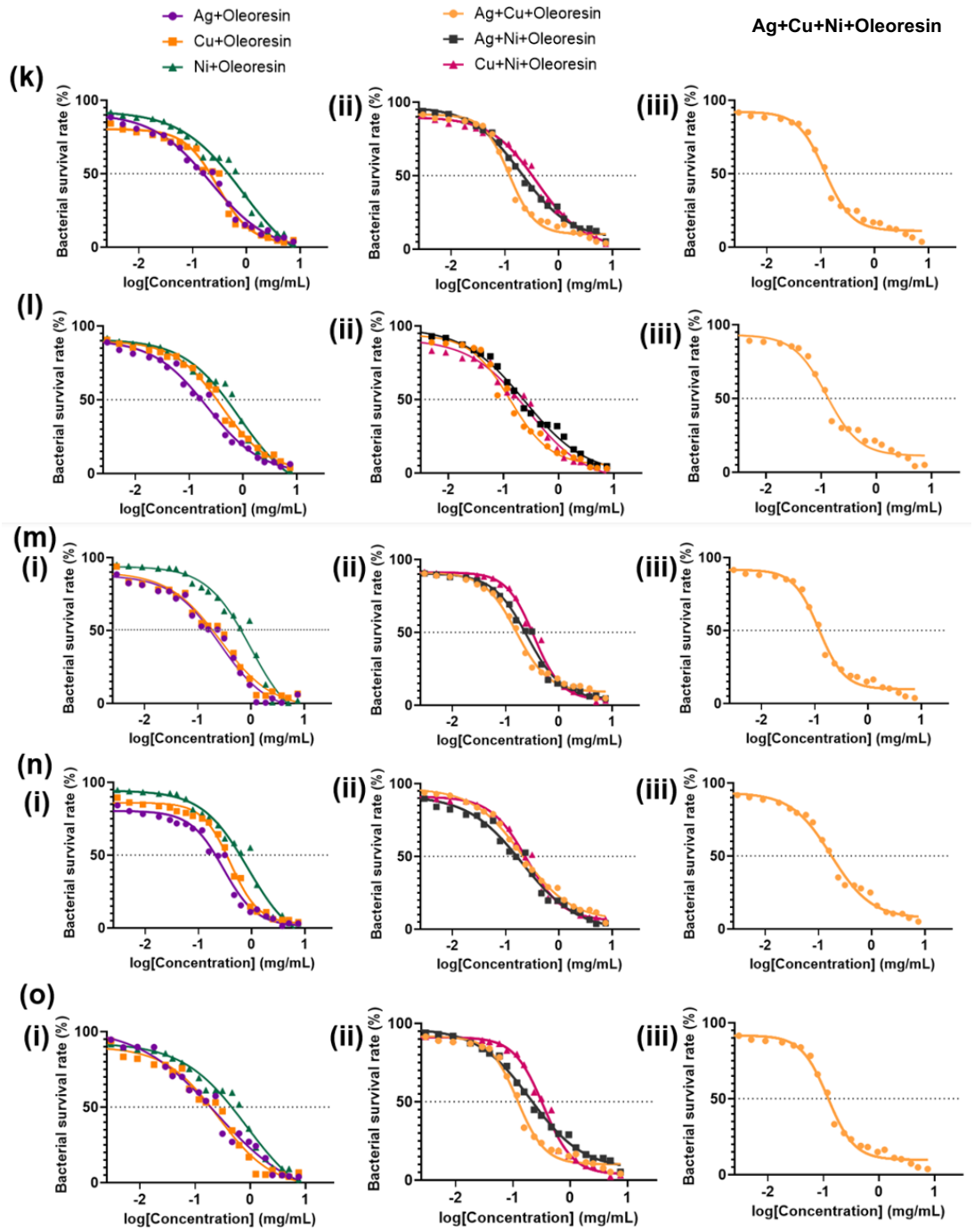

Figure S8: IC_{50} graphs of Metals only -(a) *S.aureus*, (b) MRSA (c) *E.coli* (d) *P.aeruginosa* (e) *C.albicans* ; (i) monometallic (ii) bimetallic (iii) trimetallic; Metals+curcuminoids -(f) *S.aureus*, (g) MRSA (h) *E.coli* (i) *P.aeruginosa* (j) *C.albicans* ; (i) monometallic+curcuminoids (ii) bimetallic+curcuminoids (iii) trimetallic+curcuminoids; Metals+oleoresin – (k) *S.aureus*, (l) MRSA (m) *E.coli* (n) *P.aeruginosa* (o) *C.albicans* ; i) monometallic+oleoresin (ii) bimetallic+ oleoresin (iii) trimetallic+ oleoresin.

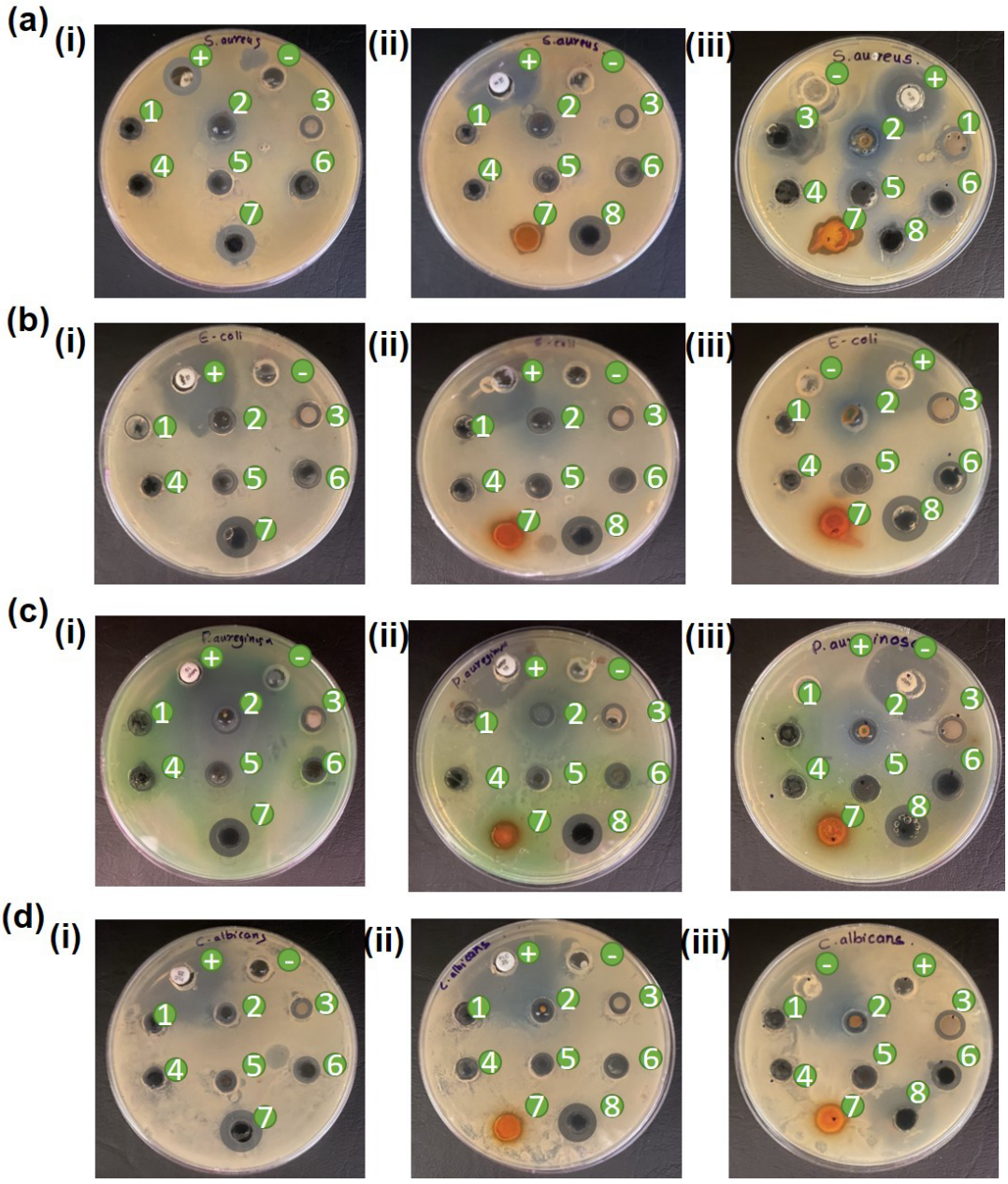

Figure S9: Well diffusion assay of (a) *Staphylococcus aureus*, (b) *Escherichia coli*, (c) *Pseudomonas aeruginosa*, (d) *Candida albicans*; (i) Inhibition zones of metallic nanoparticles; (1) Ni, (2) Cu, (3) Ag, (4) Ni+Cu, (5) Ni+Ag, (6) Ag+Cu, (7) Ag+Cu+Ni; (ii) Inhibition zones of metallic nanoparticles combined with turmeric oleoresin (TOR); (1) Ni+TOR, (2) Cu+TOR, (3) Ag+TOR, (4) Ni+Cu+TOR, (5) Ni+Ag+TOR, (6) Ag+Cu+TOR, (7) TOR (8) Ag+Cu+Ni+TOR; (iii) Inhibition zones of metallic nanoparticles combined with curcuminoids (CS); (1) Ni+CS, (2) Cu+CS, (3) Ag+CS, (4) Ni+Cu+CS, (5) Ni+Ag+CS, (6) Ag+Cu+CS, (7) CS, (8) Ag+Cu+Ni+CS, (+) Positive control, (-) Negative control – Ultrapure water (All the dispersions were 100 mg/mL of concentration and 50 µL of each solution was placed into the well).

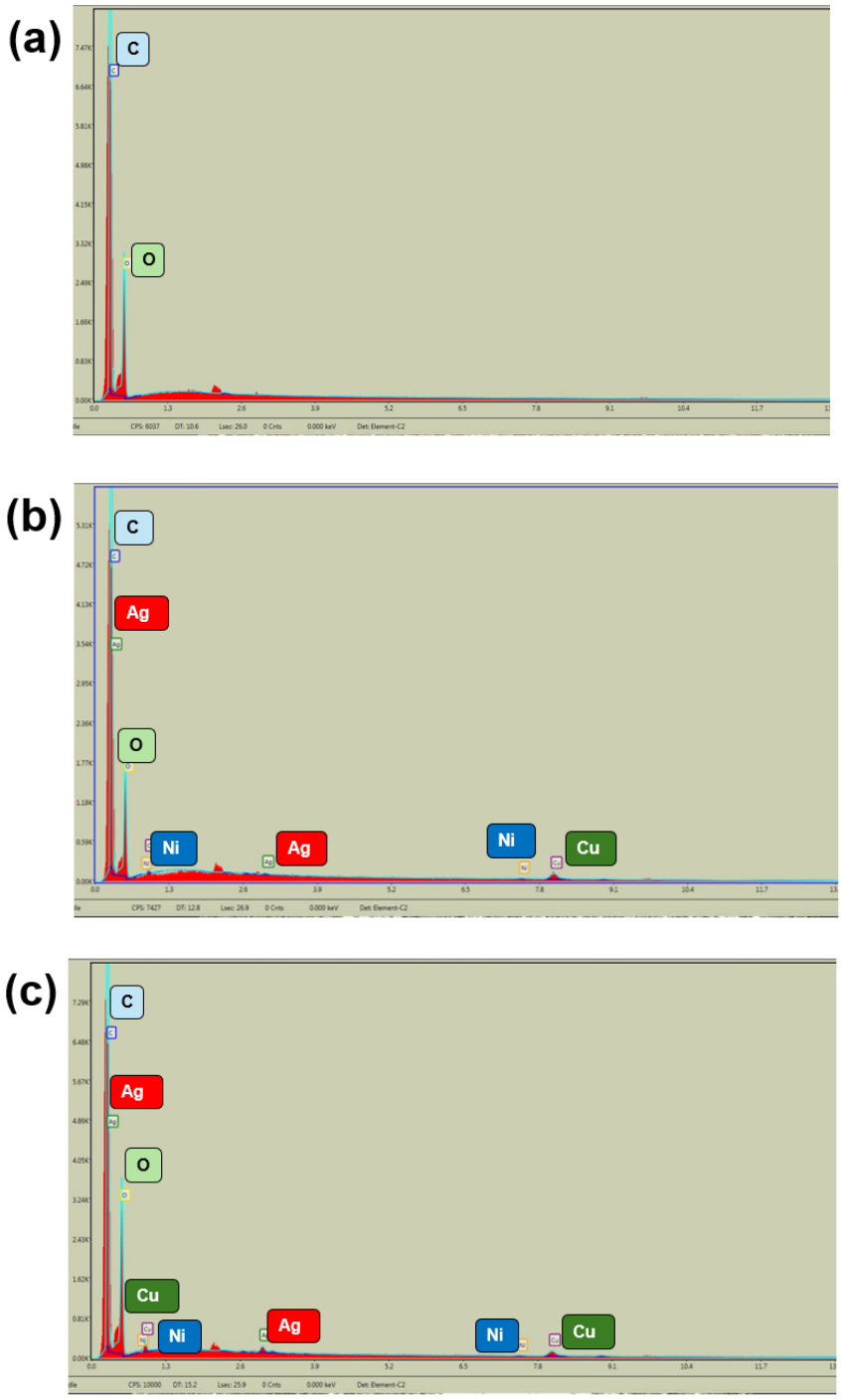

Figure S10: EDX mapping for (a) PCL mat (b) T-PCL mat and (c) T-C-PCL mat nanofiber membranes.

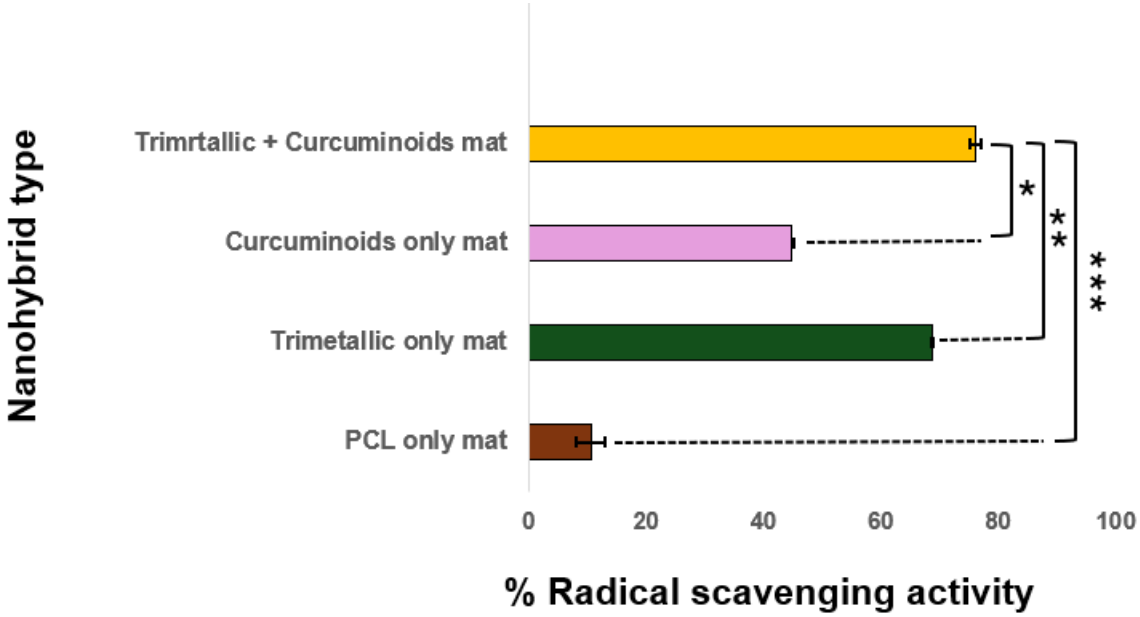

Figure S11: The % radical scavenging activities of different nanohybrids; the significant difference between, (***) trimetallic + curcuminoids mat and PCL only mat, (**) trimetallic + curcuminoids mat and trimetallic only mat, (*) trimetallic + curcuminoids mat and curcuminoids only mat.

Table S1: Synergistic antimicrobial activity of nanohybrids in combination by FICI.

Table S1.1- Synergistic antimicrobial activity of curcuminoids nanohybrids.

Type of the nanohybrid	*S. aureus*		MRSA		*E. coli*		*P. aeruginosa*		*C. albicans*	
	FICI	Synergistic activity	FICI	Synergistic activity	FICI	Synergistic activity	FICI	Synergistic activity	FICI	Synergistic activity
Ag + Cu	1.00	Adt	0.75	Syn	2.00	Atg	1.00	Adt	1.50	Atg
Ag + Ni	5.00	Atg	5.00	Atg	4.00	Atg	1.25	Atg	2.50	Atg
Cu + Ni	10.00	Atg	6.00	Atg	5.00	Atg	5.00	Atg	3.00	Atg
Ag + Cu + Ni	1.12	Adt	0.87	Atg	1.12	Adt	1.12	Adt	0.87	Syn
Ag+ Curcuminoids	1.50	Atg	1.50	Atg	3.00	Atg	3.00	Atg	1.50	Atg
Cu+ Curcuminoids	3.00	Atg	1.25	Atg	3.00	Atg	1.50	Atg	2.50	Atg
Ni+ Curcuminoids	9.00	Atg	4.50	Atg	9.00	Atg	9.00	Atg	2.25	Atg
Ag+Cu+ Curcuminoids	2.00	Atg	2.00	Atg	4.00	Atg	1.00	Adt	1.75	Atg
Ag+Ni+ Curcuminoids	6.50	Atg	6.50	Atg	6.50	Atg	8.00	Atg	4.00	Atg
Cu+Ni+ Curcuminoids	26.02	Atg	22.02	Atg	26.02	Atg	13.00	Atg	5.50	Atg
Ag+Cu+Ni Curcuminoids	1.06	Adt	0.94	Syn	1.06	Adt	1.06	Adt	0.94	Syn

Adt – Additive , Atg – Antagonist, Syn – Synergistic

Table S1.2- Synergistic antimicrobial activity of oleoresin nanohybrids.

Type of the nanohybrid	*S. aureus*		MRSA		*E. coli*		*P. aeruginosa*		*C. albicans*	
	FICI	Synergistic activity	FICI	Synergistic activity	FICI	Synergistic activity	FICI	Synergistic activity	FICI	Synergistic activity
Ag + Cu	1.00	Adt	0.75	Syn	2.00	Atg	1.00	Adt	1.50	Atg
Ag + Ni	5.00	Atg	6.00	Atg	2.50	Atg	1.25	Atg	3.00	Atg
Cu + Ni	10.00	Atg	6.00	Atg	5.00	Atg	5.00	Atg	3.00	Atg
Ag + Cu + Ni	1.12	Adt	0.87	Syn	1.12	Atg	1.12	Adt	0.87	Atg
Ag+ Oleoresin	1.50	Atg	1.50	Atg	1.50	Adt	1.50	Atg	1.50	Syn
Cu+ Oleoresin	3.00	Atg	2.00	Atg	3.00	Atg	3.00	Atg	3.00	Atg
Ni+ Oleoresin	3.00	Atg	3.00	Atg	3.00	Atg	3.00	Atg	3.00	Atg
Ag+Cu+ Oleoresin	1.25	Atg	1.37	Atg	2.50	Atg	0.62	Syn	1.37	Atg
Ag+Ni+ Oleoresin	7.00	Atg	3.50	Atg	7.00	Atg	3.50	Atg	3.50	Atg
Cu+Ni+ Oleoresin	12.00	Atg	10.00	Atg	12.00	Atg	14.00	Atg	2.50	Atg
Ag+Cu+Ni Oleoresin	1.37	Atg	1.12	Adt	1.37	Atg	1.37	Atg	2.25	Atg

Adt – Additive , Atg – Antagonist, Syn – Synergistic

Table S2- The percentage radical scavenging activity of various combinations of nanofiber mats.

Values followed by different superscripts in the same column are significantly different ($P < 0.05$) according to Tukey's pairwise comparison test (n=3)

Nanohybrid type	Radical scavenging activity (%)
PCL mat	10.59 ± 2.50^{a}
T-PCL mat	68.79 ± 0.16^{b}
C-PCL mat	44.88 ± 0.05^{c}
T-C-PCL mat	76.14 ± 0.99^{d}